REPORT DOCUMENTATION PAGE

Form Approved
OMB No. 0704-0188

Public reporting burden for this collection of information is estimated to average 1 hour per response, including the time for reviewing instructions, searching existing data sources, gathering and maintaining the data needed, and completing and reviewing the collection of information. Send comments regarding this burden estimate or any other aspect of this collection of information, including suggestions for reducing this burden, to Washington Headquarters Services, Directorate for information Operations and Reports, 1215 Jefferson Davis Highway, Suite 1204, Arlington, VA 22202-4302, and to the Office of Management and Budget, Paperwork Reduction Project (0704-0188), Washington, DC 20503.

1. AGENCY USE ONLY (Leave blank)

2. REPORT DATE: Dec 94

3. REPORT TYPE AND DATES COVERED

4. TITLE AND SUBTITLE
Toward Coherent Excitation: Development of a single-source Pump for the Rubidium Hyperfine Ground state Doublet.

5. FUNDING NUMBERS

6. AUTHOR(S)
Edward Brown Tomme

7. PERFORMING ORGANIZATION NAME(S) AND ADDRESS(ES)
AFIT Students Attending:
University of Texas at Austin

8. PERFORMING ORGANIZATION REPORT NUMBER
AFIT/CI/CIA
94-152

9. SPONSORING/MONITORING AGENCY NAME(S) AND ADDRESS(ES)
DEPRTMENT OF THE AIR FORCE
AFIT/CI
2950 P STREET
WRIGHT-PATTERSON AFB OH 45433-7765

10. SPONSORING/MONITORING AGENCY REPORT NUMBER

11. SUPPLEMENTARY NOTES

12a. DISTRIBUTION/AVAILABILITY STATEMENT
Approved for Public Release IAW 190-1
Distribution Unlimited
MICHAEL M. BRICKER, SMSgt, USAF
Chief Administration

12b. DISTRIBUTION CODE

13. ABSTRACT (Maximum 200 words)

DTIC ELECTE JAN 05 1994 S F D

19950103 049

DTIC QUALITY INSPECTED 5

14. SUBJECT TERMS

15. NUMBER OF PAGES
49

16. PRICE CODE

17. SECURITY CLASSIFICATION OF REPORT

18. SECURITY CLASSIFICATION OF THIS PAGE

19. SECURITY CLASSIFICATION OF ABSTRACT

20. LIMITATION OF ABSTRACT

94-152

ABSTRACT

Toward Coherent Excitation:

Development of a Single-Source Pump for the Rubidium Hyperfine Ground State Doublet

by

Edward Brown Tomme, M.A.

Captain, USAF

The University of Texas at Austin

1994

Coherent excitation is a phenomenon which, if achieved, could provide a new tool for the investigation of many fundamental questions in atomic physics and quantum optics. A design which could produce such coherences could lead to applications as varied as lasing without inversion and electromagnetically induced transparency. In this thesis, the basic theory concerning the generation of coherent superpositions of the ground states of atomic rubidium is reviewed. Next, the design, construction, and testing of a Littrow-style grating-tuned laser and a standing wave electro-optic modulator used in generating sidebands at the frequency matching the rubidium hyperfine ground state doublet are described. An experiment demonstrating simultaneous absorption by the ^{85}Rb F=2 and ^{85}Rb F=3 using a single laser as the pump is chronicled. An experiment to test coherences generated by this method of single-source pumping of the ground state doublet is proposed.

Accesion For
NTIS CRA&I
DTIC TAB
Unannounced
Justification
By
Distribution/
A-1

(49 Pages)

Bibliography

G.P. Agarwal and J.T. Klaus, "Effect of Phase Conjugate Feedback on Semiconductor Laser Dynamics", Opt. Lett. **16** (17), 1325, (1991).

L.B. Arguimbau and R.D. Stuart, *Frequency Modulation*, John Wiley and Sons, London, 1956.

W.F. Buell, "Semiconductor Laser Experiments with Rubidium Vapor with Applications to Fundamental and Applied Physics", Doctoral Dissertation, The University of Texas at Austin, 1994.

T.F. Gallagher *et. al.*, "Principles of a Resonant Cavity Optical Modulator", Appl. Opt. **25** (4), 510, (1986).

W.N. Hardy and L.A. Whitehead, "Split-Ring Resonator for Use in Magnetic Resonance from 200-2000 MHz", Rev. Sci. Instrum. **52** (2), 213, (1981).

I.P. Kaminow, *An Introduction to Electrooptic Devices*, Academic Press, New York, 1974.

J.F. Kelley and A. Gallagher, "Efficient Electro-Optic Modulator for Optical Pumping of Na Beams", Rev. Sci. Instrum. **58** (4), 563, (1987).

P.V. Lenzo *et. al.*, "Electrooptic Coefficients and Elastic Wave Propagation in Single Domain Ferroelectric Lithium Tantalate", Appl. Phys. Lett. **8**, 81, (1966).

K. Liu and M.G. Littman, "Novel Geometry for Single-Mode Scanning of Tuneable Lasers", Opt. Lett. **6**, 117, (1981).

P. McNicholl and H.J. Metcalf, "Synchronous Cavity Mode and Feedback Wavelength Scanning in Dye Laser Oscillators with Gratings", Appl. Opt. **24** (17), 2757, (1985).

John H. Moore *et. al.*, *Building Scientific Apparatus: A Practical Guide to Design and Construction*, 2d Ed., Addision-Wesley, Reading, Mass, 1989.

J. Sabbaghzadeh, "A Highly Sensitive Spontaneous Raman Spectrometer for the Determination of Concentrations in Gas Mixtures", 1993, unpublished.

Marlan O. Scully, "From Lasers and Masers to Phaseonium and Phasers", Physics Reports **219** (3-6), 192, (1992).

Copyright

by

Edward Brown Tomme

1994

Toward Coherent Excitation:

Development of a Single-Source Pump for the Rubidium Ground State Hyperfine Doublet

by

Edward Brown Tomme, B.S.

Thesis

Presented to the Faculty of the Graduate School

of The University of Texas at Austin

in Partial Fulfillment

of the Requirements

for the Degree of

Master of Arts

The University of Texas at Austin

December 1994

Toward Coherent Excitation:

Development of a Single-Source Pump for the

Rubidium Ground State Hyperfine Doublet

APPROVED BY

SUPERVISORY COMMITTEE:

Manfred Fink

Manfred Fink

John Keto

John Keto

To my best friend, Tracey.

ACKNOWLEDGEMENTS

Almost two years ago when I was taking an experimental physics course, I was approached by Dr. Wally Buell, then a graduate student working for Professor Manfred Fink. He and Dr. Fink had an idea for trying to write sidebands on an external cavity laser, the project which eventually became the basis for this thesis. Dr. Buell's energy, his seemingly inexhaustible supply of theoretical knowledge, and his unparalleled ability to push diode laser technology to its limits were, in a great degree, the only reason this project ever left the pages of technical journals. Although he has since become a post-doctoral assistant at the State University of New York at Stony Brook, Wally continues to be a daily inspiration and source of wisdom for me.

Professor Manfred Fink had his own way of motivating me to become a professional physicist. I owe much of my technical knowledge to his policy of scientific *laissez-faire*. As a mere graduate student, he gave me the opportunity to completely control my project, including dedicating reasonably large sums of money and considerable equipment at will. I understand substantially more about how the lasing without inversion and electromagnetically induced transparency phenomena do and don't work due to the many lengthy discussions that we shared. I also understand a great deal more about the narrow tightrope that a truly successful scientist must walk between being an effective manager, being a superlative showman, and

sometimes even squeezing in the time to do real science every once in awhile. Manfred is a scientist's role model without peer.

There are many others whose guidance, suggestions, and even casual remarks allowed this project to proceed. Although by no means an all-inclusive list, I do owe debts of thanks to Mr. Terry Cole, Major Randy Correll, Ms. Thien Trang Dang, Mr. Joe Holder, Professor John Keto, Mr. Bruce "Skippy" Klappauf, Mr. Bob Earl LaFon, Mr. Mike Matthews, Mr. Ed McKnight, Dr. Fred L. Moore, Mr. Pat Morrow, Mr. Jim Pinget, Professor Mark Raizen, Mr. Jamshid Sabbaghzadeh, Mr. Brad Shadwick, and Mr. Leif "Chip" Thuesen. Each of these people had their own contribution to this design. I also owe thanks to Jim Mitchell and Troy Rodriguez at Sierra Microwave Technology in Georgetown, Texas, for the generous donation of several expensive RF isolators and circulators for this project, as well as enlightening discussions on RF circuitry in general.

Special thanks go to Mr. John Robinson, who graciously stepped in as my local source of technical knowledge after Dr. Buell's departure; the long hours he spent helping me tweak the electro-optic modulator saved me weeks of effort on my own. Most of all, I thank my wife, Tracey, for understanding my long hours and still being there when I needed her.

December, 1994

ABSTRACT

Toward Coherent Excitation:

Development of a Single-Source Pump for the Rubidium Hyperfine Ground State Doublet

by

Edward Brown Tomme, M.A.

The University of Texas at Austin, 1994

SUPERVISOR: Manfred Fink

Coherent excitation is a phenomenon which, if achieved, could provide a new tool for the investigation of many fundamental questions in atomic physics and quantum optics. A design which could produce such coherences could lead to applications as varied as lasing without inversion and electromagnetically induced transparency. In this thesis, the basic theory concerning the generation of coherent superpositions of the ground states of atomic rubidium is reviewed. Next, the design, construction, and testing of a Littrow-style grating-tuned laser and a standing wave electro-optic modulator used in generating sidebands at the frequency matching the rubidium hyperfine ground state doublet are described. An experiment demonstrating

simultaneous absorption by the ^{85}Rb F=2 and ^{85}Rb F=3 using a single laser as the pump is chronicled. An experiment to test coherences generated by this method of single-source pumping of the ground state doublet is proposed.

TABLE OF CONTENTS

LIST OF FIGURES x

CHAPTER ONE: INTRODUCTION 1

CHAPTER TWO: THEORY 4

CHAPTER THREE: APPARATUS 7

THE GRATING-TUNED LASER 9

THE ELECTRO-OPTIC MODULATOR 14

CHAPTER FOUR: EXPERIMENTAL PROCEDURE 24

EQUIPMENT EVALUATION 24

THE SIMULTANEOUS PUMPING EXPERIMENT 35

CHAPTER FIVE: FUTURE WORK 44

BIBLIOGRAPHY 46

VITA 49

LIST OF FIGURES

Figure 1: Hyperfine Energy Levels of the Rubidium D_1 and D_2 Transitions . . . 2

Figure 2: Energy Level Diagrams of Two Types of Systems for Observing Coherent Effects 4

Figure 3: The Littrow and Littman Grating-Tuned Laser Designs 10

Figure 4: Photograph of the Grating-Tuned Laser 12

Figure 5: Schematic of the Electro-Optic Modulator 15

Figure 6: Relative Carrier and Sideband Magnitudes for Various Modulation Indices 17

Figure 7: Photograph of the Plastic Crystal Mount 21

Figure 8: Laser Output Power vs. Injection Current 25

Figure 9: RF Oscillator Frequency vs. Tuning Voltage 28

Figure 10: Photograph of The Experimental Setup 29

Figure 11: Tube Size vs. Resonant Frequency 32

Figure 12: Optical Spectrum Showing the Laser Carrier and Sidebands 33

Figure 13: Time Dependence of EOM Resonant Frequency 34

Figure 14: The Rubidium D_2 Absorption Spectrum 36

Figure 15: Simultaneous Absorption While Tuned to the ^{85}Rb F=2 Transition 38

Figure 16: Simultaneous Absorption While Tuned to the 85Rb F=3 Transition. 40

Figure 17: Absorption with the Carrier Slightly Off the ^{85}Rb F=2 Resonance 41

Figure 18: The Rubidium Absorption Spectrum With and Without Sidebands 42

CHAPTER ONE: INTRODUCTION

The advent of inexpensive, narrow linewidth optical sources such as diode lasers reawakened the field of atomic and molecular physics, making possible many previously impractical or impossible explorations. One of these areas was the question of coherent states of matter. Which new phenomena lay waiting to be discovered if one could cause atoms to exist in a coherent superposition of their atomic states? Several researchers have shown that should such superpositions be achieved, they could be the basis for diverse projects from enormously improved microscopes to lasers that do not require the normal population inversion for the gain mechanism.

A coherent superposition implies that two distinct atomic states are driven in such a manner that they cease to exist as individual units and instead exist together in a new, normally unreachable state. For the purposes of this thesis, the coherent superposition we will choose to examine will be a superposition of the ground states of rubidium. An alkali metal with a reasonably well understood atomic structure, rubidium has a ground state that consists of two hyperfine states split by a small energy difference, as is shown in Figure 1[1]. The goal will be to generate Rabi oscillations between the ground state doublet and the $5P_{3/2}$ excited state (on resonance

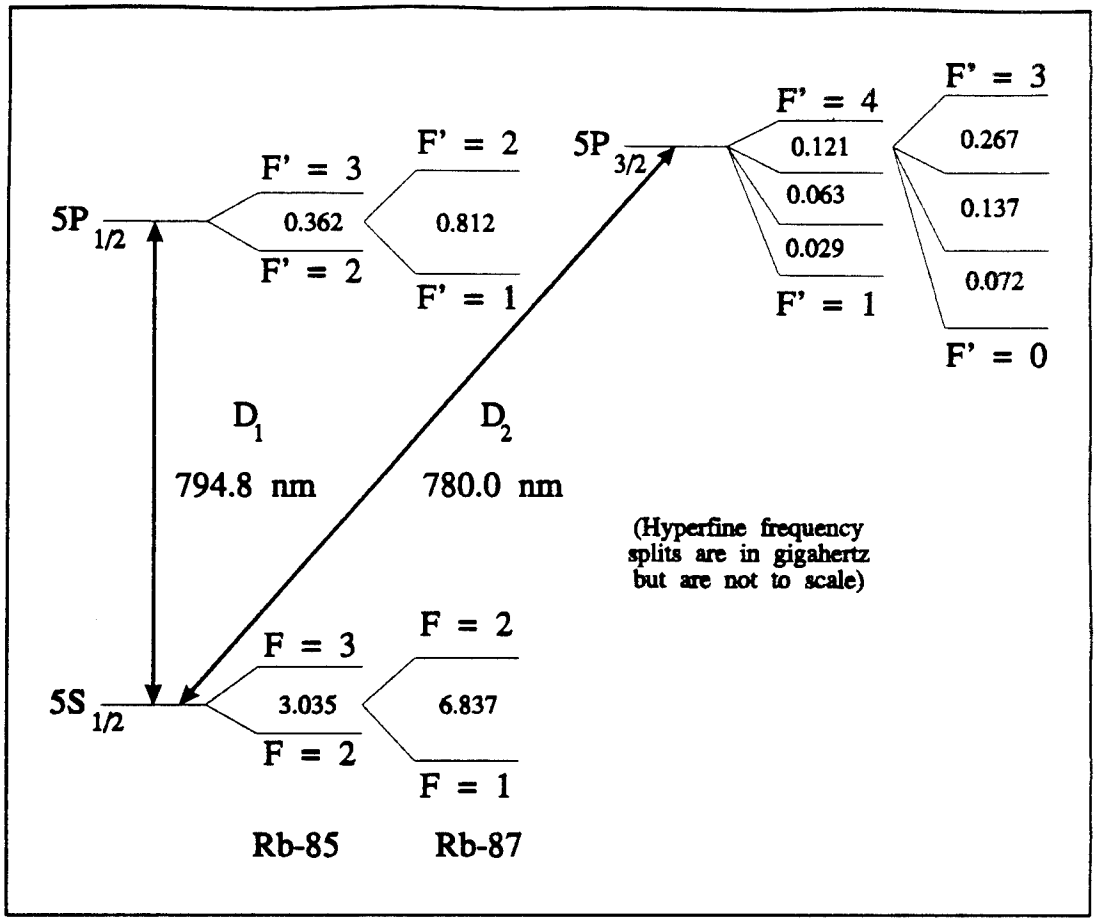


Figure 1: Hyperfine Energy Levels of the Rubidium D_1 and D_2 Transitions. Note that the hyperfine energy splittings are not necessarily symmetric about the base energy.

with approximately 780 nm photons) using the same pumping source. For two reasons, our work will concentrate solely on the rubidium 85 isotope: the natural abundances of the rubidium isotopes are 72.1% ^{85}Rb and 27.9% ^{87}Rb, and most of the equipment we will use has an upper frequency limit of about 4 GHz.

The use of one source to pump the doublet simultaneously will require the use of leading edge technology for laser linewidth control, frequency control, and novel

radio frequency sideband generation techniques. A single diode laser will be aligned in an external diffraction grating cavity using the Littrow technique. The laser will then be tuned and locked to one of the absorption lines of ^{85}Rb. The laser beam will then be directed into an electro-optic modulator which will be driven at the frequency of the doublet's energy separation. The electro-optic modulator will thus generate FM sidebands, one of which will lie at the absorption line of the other component of the doublet. When the laser is passed through a cell containing rubidium gas, the gas will absorb energy from both the optical carrier and the sideband. Coherence will be achieved when the phases of the carrier and sideband match once every period of the beat frequency of the two absorption frequencies.

As can be readily seen, each of the fundamental steps required to be mastered before even attempting to achieve a coherent superposition of states is in itself a formidable task. In the following chapters, we will more closely examine the underlying theory of coherent excitation, the methods used in this particular research, and several directions for further work in this field.

CHAPTER TWO: THEORY

Coherent excitation is not a new idea. For many years, theoretical physicists have developed models of systems for which they expected to observe coherent effects. The two most widely used models both involve three atomic energy levels and have quite descriptive names. The first model is called the V system, so named because it normally involves an excited state doublet and a far-removed ground state. The second coherence model involves a ground state doublet and is therefore called the Λ model. Figure 2 schematically depicts the energy diagrams for both of these schemes. In this figure, the levels labelled A and A' are the doublet and B is the far-removed state. The wavelengths λ_1 and λ_2 couple the doublet with the excited (or ground) state. The dotted energy level represents a possible location for a coherent superposition of the doublet states; λ_3 is the wavelength which will induce the transitions from the superposition state to the far-removed state.

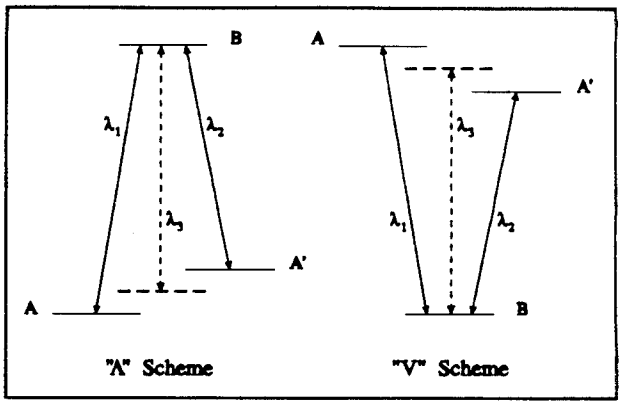


Figure 2: Energy Level Diagrams of Two Types of Systems for Observing Coherent Effects.

Following an argument by Scully[2], For a Λ type system with a laser tuned to λ_3, the probability of absorption is only proportional to the density of atoms in states A and A' and the intensity of the stimulating electromagnetic radiation, or

$$P_{absorp} \propto E^2(\rho_{AA} + \rho_{A'A'} + \rho_{A'A} + \rho_{AA'}) \quad , \tag{1}$$

assuming the couplings between each element of the doublet and the excited state are equal. The probability of stimulated emission is proportional only to the density of atoms in the excited state B and the electromagnetic intensity, or

$$P_{emission} \propto E^2 \rho_{BB} \quad . \tag{2}$$

Thus, the gain (or attenuation) in the stimulating electromagnetic field is proportional to the probability of absorption minus the probability of emission

$$\dot{E} \propto E(\rho_{BB} - \rho_{AA} - \rho_{A'A'} - \rho_{A'A} - \rho_{AA'}) \quad . \tag{3}$$

If we are able to tune the wavelength of the stimulating laser in such a manner that the matrix elements coupling the doublet exactly cancel the doublet elements themselves, the gain will be proportional only to the density of atoms in the excited state. A normal gain equation depends on a population inversion, that is, the excited state must have more atoms available to emit than the ground state has atoms to absorb. In the coherent scheme, the gain depends only on the *total* number of atoms in the excited state, so lasing can begin at much lower excited state densities. This is known as lasing without inversion.

Another application of this coherence generation is the cancellation of absorption. This phenomenon is simply the above argument, neglecting the stimulated emission portion. If the coupling matrix elements exactly cancel the pure state elements in equation (1), the probability of absorption will be zero. This means that a weak probe beam of wavelength λ_1 or λ_2 that transits an area where the coherences are generated by a strong pump laser will not be absorbed. The importance of this effect becomes apparent when one notes that the index of refraction is normally quite high in the area of a resonance.[3] An electromagnetic field that can propagate unabsorbed in an area of high index of refraction would be a boon to microscope designers.[4] Since the resolving power of a microscope is proportional to the index of refraction of the fluid in which the sample lies, the higher the index, the better the microscope. Traditional microscopes attempt to use a higher index by immersing the subject and the lens in a transparent oil, however the resolution enhancement of this technique is minuscule when compared to the enhancement possible when the microscope operates in a region of electromagnetically induced transparency.

Although this has been a very basic discussion of the relevance of coherent stimulation, hopefully it will be enough to motivate the reader to continue on with this tome. In the next chapter we will discuss the particular method with which we chose to generate the coherences.

CHAPTER THREE: APPARATUS

Now that the basics of some of the theories behind coherent excitation and some of its ramifications have been explained, it is time to move from the abstract to the concrete. Probably the most difficult part of the entire project was the design, construction, and testing of several pieces of precision equipment.

In order to generate the coherent couplings required in the experiment, it is necessary to pump two discrete energy states in such a manner as to allow at least a part-time phase matching of the pumping sources. There were several ways to achieve this goal. First, two distinct lasers tuned to the individual absorption lines could be phase-locked to provide a partially coherent source. Second, an RF signal could be coupled to the injection current of a single diode laser, causing sidebands to appear on the laser beam at the proper frequency difference to pump both states in the ground state doublet. Third, a single diode laser beam could be directed through an electro-optically active crystal causing similar sidebands to appear.

The first scheme had in its favor the simplicity of only having to tune two diodes to relatively independent frequencies, and then use the relatively well-understood technique of injection locking to keep their phases from wandering too far apart. The biggest disadvantage came as a result of the existence of two independent

beams. Trying to align such a setup so that the beams interacted with the same spatial region in the test area while they did not interfere with each other in the detection area is difficult. Since we were anticipating using the apparatus for long time periods where any interruption would be disastrous to a larger experiment, the inherent instability of copropagating or counterpropagating beam designs was deemed to be an overwhelming negative.

The second scheme, dithering the diode injection current at RF frequencies, was also rejected. First, the ability of currently available diode lasers to predictably respond to a high frequency dithering on the order of the semiconductor carrier lifetimes had not been completely explored. Whether the semiconductors could even respond that quickly with the required precision was a matter of discussion. Additionally, in order to achieve large amplitude, tuneable sidebands with such a scheme, we would have to design our grating-tuned laser to have an external cavity which was resonant at both the RF and the laser frequency. This increase in complexity was deemed to be very risky.

After rejecting these two approaches, we finally decided to use the third scheme, the one that depended upon the electro-optic modulator (EOM) for the sideband generation. Although this method involved the building of an additional piece of completely different equipment than was required for either of the other two designs, it had the advantage of being a technique that was currently successfully

being used by another group here at The University of Texas. Unfortunately, their EOM and all of the papers upon which it was based were using frequencies far lower than the ones we would need for the rubidium hyperfine splitting.

THE GRATING-TUNED LASER

After the basic plan of attack was determined, it remained to design and construct the requisite equipment. The first order of business was to construct a tuneable laser. As previously mentioned, this laser would be locked to one of the absorption lines of ^{85}Rb. Diode lasers are relatively easily tuned without a great deal of attendant equipment. The lasing frequency is highly dependent upon not only the temperature of the diode (a relation of approximately 30 GHz per Kelvin) but upon the injection current being fed to the diode (a relation of approximately -3.6 GHz per milliamp in the linear region of the L-I plot)[5]. However, for long-term experiments where a stable frequency output is desired, it is difficult to change these parameters quickly enough to accurately lock the laser.

A much more effective passive method of frequency-locking a diode laser has proven to be the use of selective feedback from the laser output to self-lock the laser. This method not only locks the laser, but has the additional benefit of significantly narrowing the laser linewidth[6]. One widely used method of obtaining this selective

feedback is based on using a moveable diffraction grating to form an extended cavity which selects the frequency of feedback.

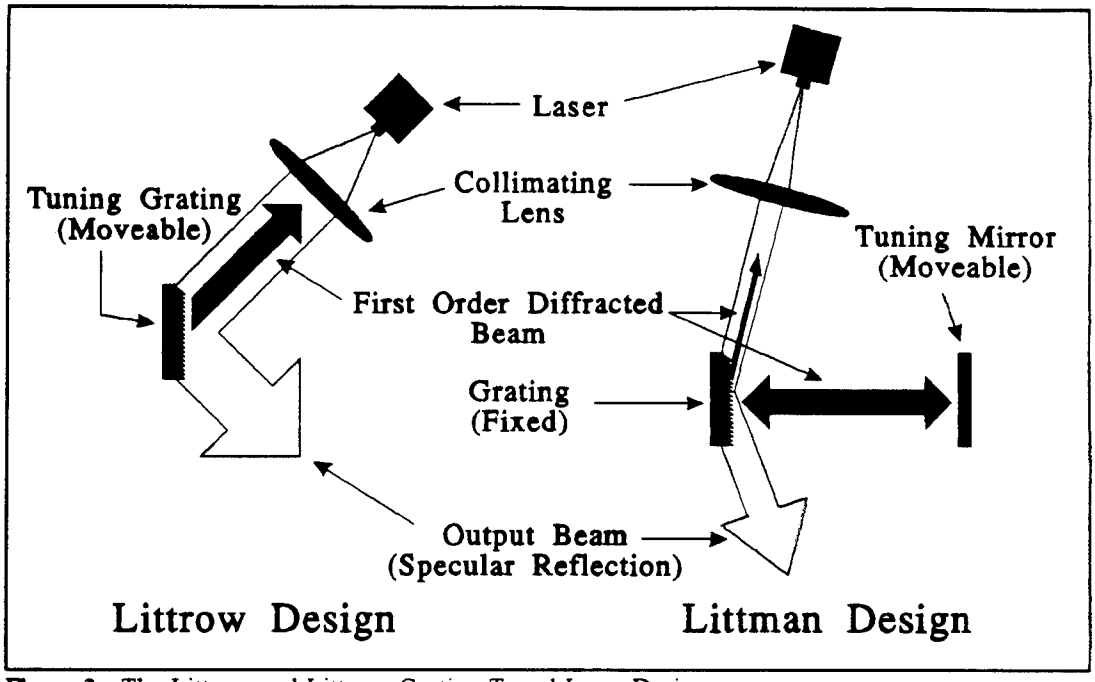


Figure 3: The Littrow and Littman Grating-Tuned Laser Designs.

There are currently two popular methods which achieve this feedback stabilization: the Littrow method and the Littman design. Note that both methods require that the front facet of the diode laser carry a high quality anti-reflection coating. In the Littrow method[7], the grating angle is chosen so that the angle of incidence is exactly equal to the angle of diffraction for the first order peak from the grating (see Figure 3). Thus, photons from the first order peak return to the laser diode where they stimulate additional photons of the same frequency. This preferential gain quickly results in a noticeable linewidth narrowing of the output

beam. In addition to ensuring the angle of diffraction feeds the desired frequency back into the laser, the distance from the laser rear facet and the grating must also be properly designed so that the laser external cavity resonates at the exact frequency selected by the grating dispersion. The trick to designing an effective Littrow system is to ensure that when the grating is rotated to feed a different frequency back into the laser, the external cavity length is changed by a commensurate amount. Failure to do so will result in a mode-hop and a fairly short continuous tuning range.

The Littman method is a more complex setup[8], but offsets its complexity by allowing a much greater frequency selectivity than the Littrow design. In this design, a moveable mirror provides the tuning mechanism. The first order peak from the grating is directed to the mirror, where it is reflected back to the grating, diffracted again, and then fed back into the laser. The typically longer external cavity lengths and the fact that the feedback beam is diffracted twice provide the greater tuning frequency resolution. It has also been shown that for the Littman design there exists an optimum relation between the location of the grating plane, the mirror plane, the front facet of the laser, and the axis of rotation which will exactly match the grating rotation to the cavity length change, resulting in extremely large continuous tuning ranges.[9]

When this project was first envisioned, we were much more familiar with the Littrow design, as another group here at The University of Texas was successfully

employing the system, so that method was chosen as the design of preference. In hindsight, the advantages of the Littman design probably would make it a better suited for our needs.

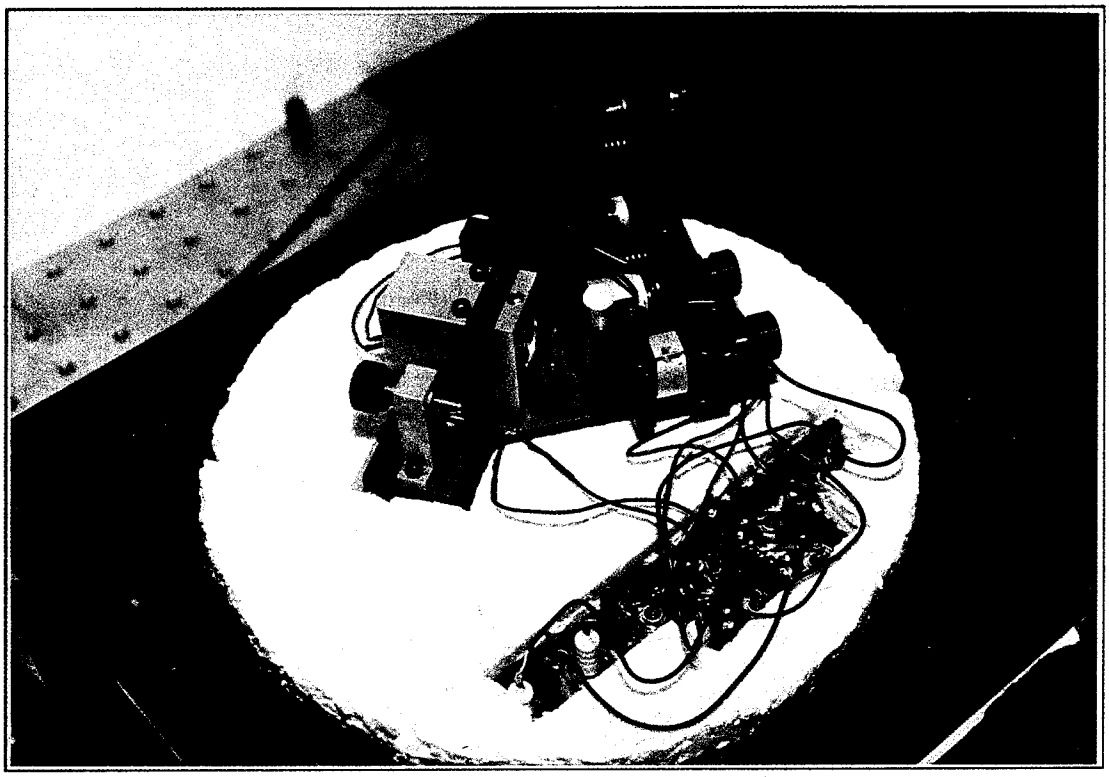


Figure 4: Photograph of the Grating-Tuned Laser. See text for details.

Photographs of the grating-tuned laser we used are shown in Figure 4. The small aluminum box at the left of the photo contains the laser diode. The adjustment screw beside that box adjusts the focus of the collimating lens, which is mounted in the aluminum holder to the right of the laser diode. The grating is held in place by the white nylon screw at the center of the picture. The two silver-colored objects to the right and above the grating are cylindrical piezo-electric crystals with which the

laser feedback is tuned. To the right of the cylinders are three adjustment screws for fine-tuning the grating tilt.

This laser is a modification of a design first used by M. Matthews while working for the D. Heinzen group at The University of Texas at Austin. This design allows the option of choosing either a four- or an eight-centimeter cavity. We chose the shorter cavity to increase the cavity mode spacing and to decrease the possibility of mode hops during tuning. The grating we used was a very high quality Thermal Jarrell Ash reflection grating with 1180 lines per millimeter. After initial testing with several inexpensive, low-power laser diodes, we chose the Hitachi HL7851G laser diode for use in the coherent excitation scheme. This laser has a nominal CW output power of 50 mW and a nominal room temperature wavelength of 785 nm. A Marlow Industries DT1089 thermoelectric cooler provides temperature stabilization of the laser diode assembly and the cavity base. The two piezo-electric cylinders provide gross- and fine-tuning of the cavity length. Control of the piezos is provided by a home-built high-voltage amplifier based on a National Institute of Standards and Technology circuit design.

The most important part of successfully getting a grating-tuned laser to frequency-lock is proper beam collimation, thus alignment was our first concern. To this end, the grating support structure and the laser housing were removed so an undeflected beam was available for testing. The beam was focused on a wall

approximately ten meters from the laser and the collimating lens was carefully adjusted to ensure that the beam passed through and normal to the center of the lens to minimize aberrations. This was accomplished by manually moving the collimating lens so that the beam was parallel to the floor and so that it did not diverge horizontally from the longitudinal axis of the diode. The beam was then focused so that the beam size remained approximately constant across the room. Results of initial testing and evaluation of the grating-tuned laser are presented in the next chapter.

THE ELECTRO-OPTIC MODULATOR

As the grating-tuned laser was designed to be able to keep the laser tuned to the frequency of one of the rubidium absorption lines, the electro-optic modulator needed to generate sidebands separated from the carrier frequency by the exact split between the two ^{85}Rb lines. Several researchers[10,11,12] have reported methods for optical sideband generation in the RF modulation range, but no working models have been demonstrated at frequencies as high as are required for the rubidium frequency split.

Following Gallagher's approach[10], we decided to employ a lumped LRC circuit

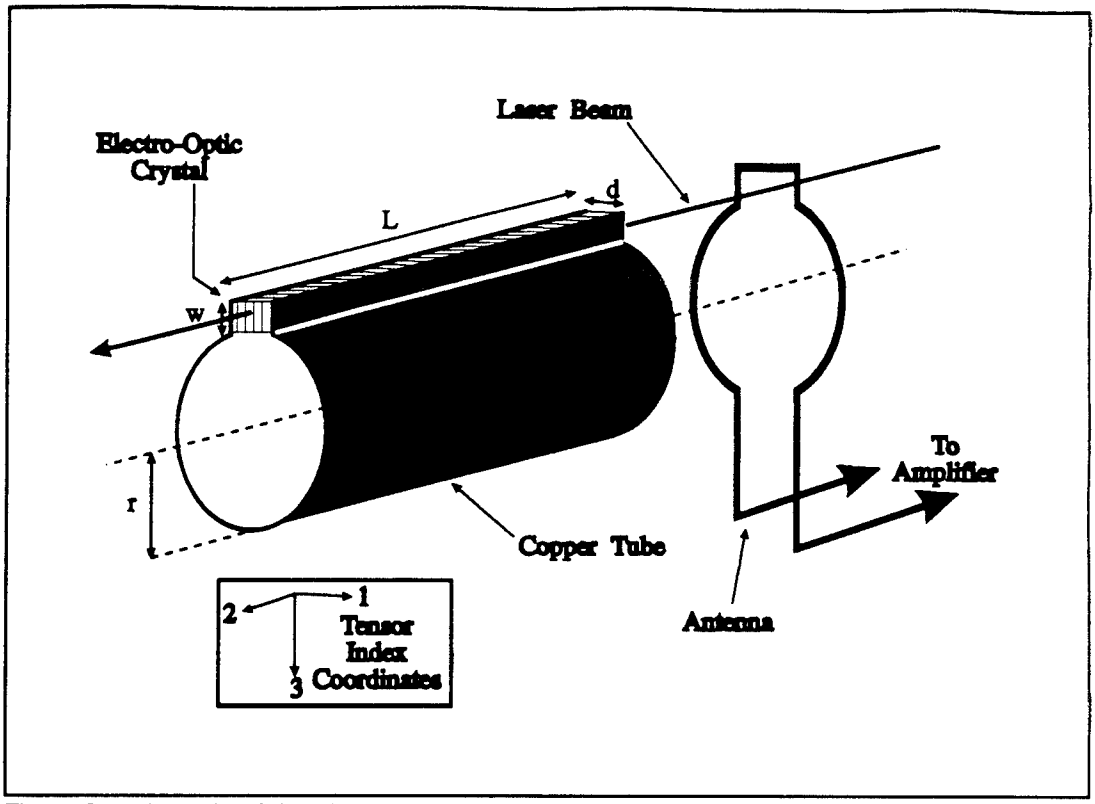


Figure 5: Schematic of the Electro-Optic Modulator.

design using the electro-optically active crystal lithium tantalate ($LiTaO_3$). This design relies on a conducting tube that is split longitudinally to house the electro-optic crystal, as shown in Figure 5. A loop antenna is then brought in proximity to the conducting tube and RF energy is coupled into the LRC circuit through this antenna. As the input RF energy is tuned to the natural resonance of the tube/crystal circuit, large voltage oscillations are generated across the crystal. These voltage oscillations cause the index of refraction within the crystal to vary. The change in index causes a local change in the velocity of light. Thus, when a laser is directed through the

crystal, this periodic index variation causes phase modulation sidebands (which are equivalent to frequency modulation sidebands[13]) to appear on the laser beam at multiples of the driving RF frequency.[14]

In general, the amplitude of FM sidebands depends upon Bessel functions with an argument known as the modulation index.[15] The FM spectrum generated by such an arrangement is given by[16]

$$E(t) = E_0 \sin(\omega_0 t + \beta \sin \omega_m t)$$
$$= E_0 \sum_{n=-\infty}^{\infty} J_n(\beta) \sin(\omega_0 + n\omega_m)t \qquad (4)$$

where ω_0 is the optical frequency, ω_m is the RF modulation frequency, β is the modulation index, and J_n is the nth order Bessel function. For our application, we would like as much of the energy as possible to be directed into the first-order sideband so that the sideband and the carrier intensities have similar orders of magnitude. Figure 6 shows plots of relative intensities of the sidebands as a function of the modulation index. This series of calculations indicates that the optimal modulation index would be on the order of 1.5.

The modulation index of an electro-optic crystal is given by the relation[17]

$$\beta_{ij} = \pi L n_i^3 r_{ij} E_j / \lambda_0 \, . \qquad (5)$$

In this equation, L is the crystal length, n_i is the index of refraction for light polarized in the ith direction, r_{ij} is the linear electro-optic coefficient tensor element, E_j is the

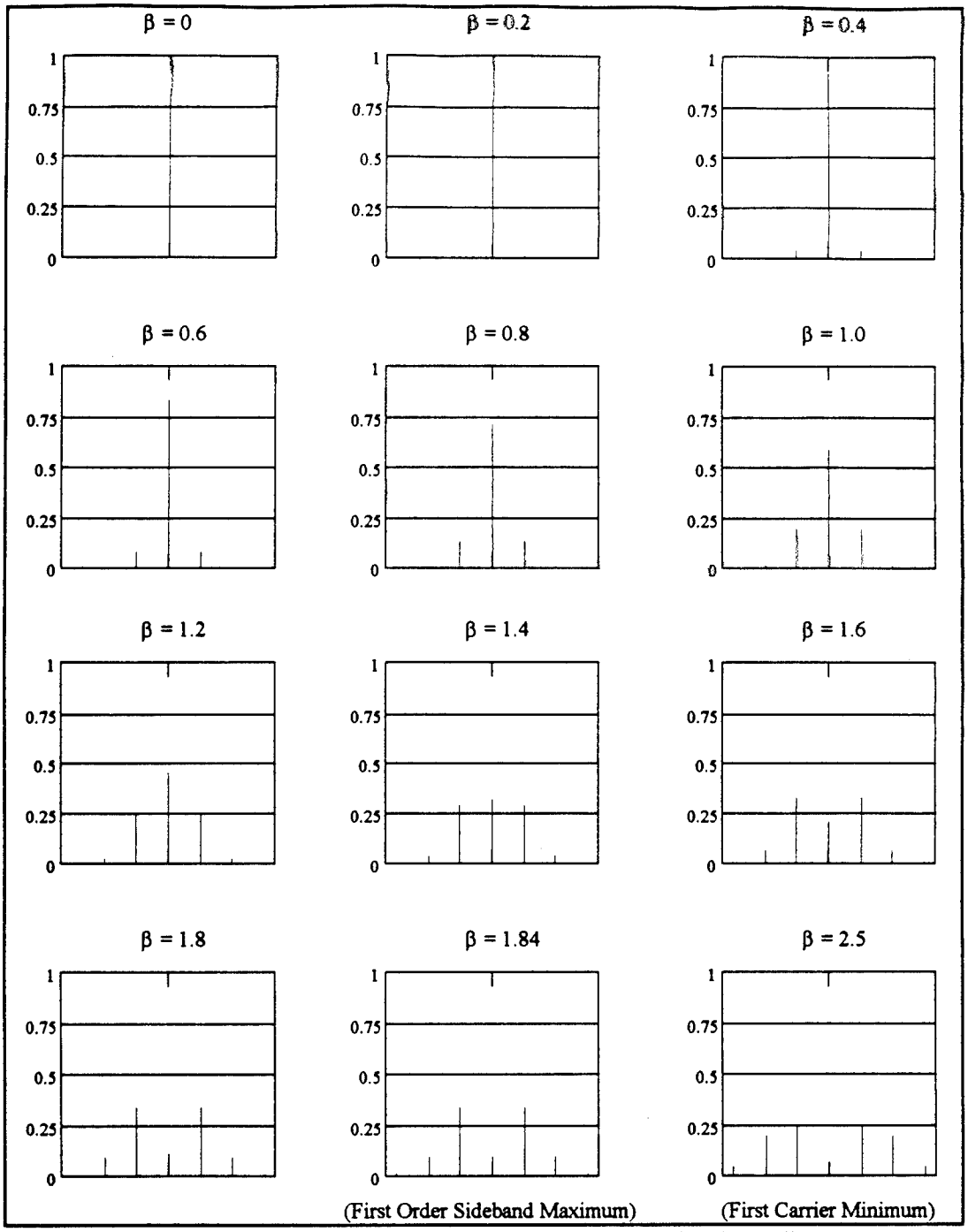


Figure 6: Relative Carrier and Sideband Magnitudes for Various Modulation Indices.

modulating electric field applied along the jth crystal axis and λ_0 is the wavelength of the optical field.

Examining this equation, it is obvious that to reach a high modulation index, one must maximize n_i, r_{ij}, L and E_j. Our choice of $LiTaO_3$ has done a good job of maximizing the first two parameters. For this substance, n_3 at an optical field wavelength of 600 nm is about 2.188 and r_{33} is about 30.3 x 10^{-12} m/V at 633 nm and a modulation frequency of 75 MHz.[18] Note that neither of these values were taken at the wavelengths or the modulation frequencies required in our experiment; we failed to discover values of these parameters at other wavelengths and many crystal manufacturers[19,20,21] seem to use these very figures during the development of products designed for a wide variety of frequencies.

The crystal length is not an entirely free parameter. In $LiTaO_3$, the phase velocity of the RF wave is about three times slower than that of the optical wave. Thus, if the crystal length approaches the RF wavelength, phase velocity matching considerations will become a significant design problem.[22] At 3 GHz, the wavelength is on the order of 100 mm, so to avoid phase matching complications we decided to limit the length of our crystal to 30 mm.

The only remaining free parameter we have is the amplitude of the electric field applied across the crystal. Our use of a resonant LRC circuit will maximize the field amplitude while keeping the device's power consumption down to reasonable

levels; a resonant circuit of reasonably high quality will produce a sharp spike in the electric field amplitude when the modulating frequency is tuned to the natural resonance of the circuit.

To calculate the resonant frequency of a lumped LRC circuit of the kind used in this experiment, we must first make several simplifying assumptions[23] (refer to Figure 5 for the relevant dimensions). First, we assume that the lumped LRC circuit is a valid approximation. This is justified since the relatively high dielectric constant of $LiTaO_3$ causes the electric field within the crystal to behave as if the crystal were an ideal capacitor. Secondly, we will model the EOM as a long ($L \gg r$), simple cylinder. This implies that the gap filled by the crystal must be small compared to the circumference, or $d \ll 2\pi r$. Finally, the crystal's dielectric constant tensor is not well known at non-zero modulation frequencies (values other than dc). The manufacturers cited above use the dc value[24] of ε_3, 0.38×10^{-9} f/m (implying that $\varepsilon/\varepsilon_0 \approx 43$), for designing these devices. Taking into account these assumptions, the resonant frequency of such a lumped LRC circuit is found from[25]

$$f_{res} = \frac{1}{2\pi}\left(\frac{c}{r}\right)\left(\frac{d}{\pi w}\right)^{1/2}\left(\frac{\varepsilon_0}{\varepsilon(\omega_m)}\right)^{1/2}. \qquad (6)$$

Several factors influenced our choices of the remaining two crystal dimensions. In order to make the construction of the tube reasonably easy, we decided to limit the tube diameter to no less than 5 mm. This choice forced the ratio of w-to-d, the

crystal's width and the depth, to be 0.293 in order to get a resonant frequency of 3.035 GHz. In order to satisfy the ideal cylindrical LRC circuit assumption mentioned above, we needed to keep d as small as possible, however we still needed to have w large enough to make laser beam alignment reasonably simple and also large enough that the 30 mm long crystal would be structurally sound. We decided that we can focus our beam onto an area slightly less than a millimeter on a side, so the final crystal dimensions chosen were (x, y, z) = (0.88, 30, 3) mm, where x, y, and z correspond to the tensor indices 1, 2, and 3.

The conducting tube was constructed from a sheet of 5 mil Olin ETP annealed copper alloy #110, which is 99.9% pure copper. Care was taken to ensure that during construction the copper was not scratched and that contaminants which could lead to corrosion were completely removed. These precautions help to maximize the Q of the cavity. The copper sheet was cut to the proper dimensions and was carefully bent to the desired shape. First, the long, straight tabs that were to abut the crystal were bent up along the edges of the sheet. Next, the sheet was wrapped around a drill bit of the appropriate size to form the cylindrical tube. The simplicity of this construction scheme is one of the reasons that values of the material constants for $LiTaO_3$ far from the target RF and optical frequency values can be accepted; the tube simply cannot be made precisely enough for the (presumably) small errors in those values to have a major effect. Other researchers[26] have gone to much greater effort preparing the

surface between the crystal and the tabs, and their efforts have been rewarded by slightly higher modulation index values than this technique provided. However, for the purposes of this experiment, this much simpler, much less time consuming method produced quite acceptable results.

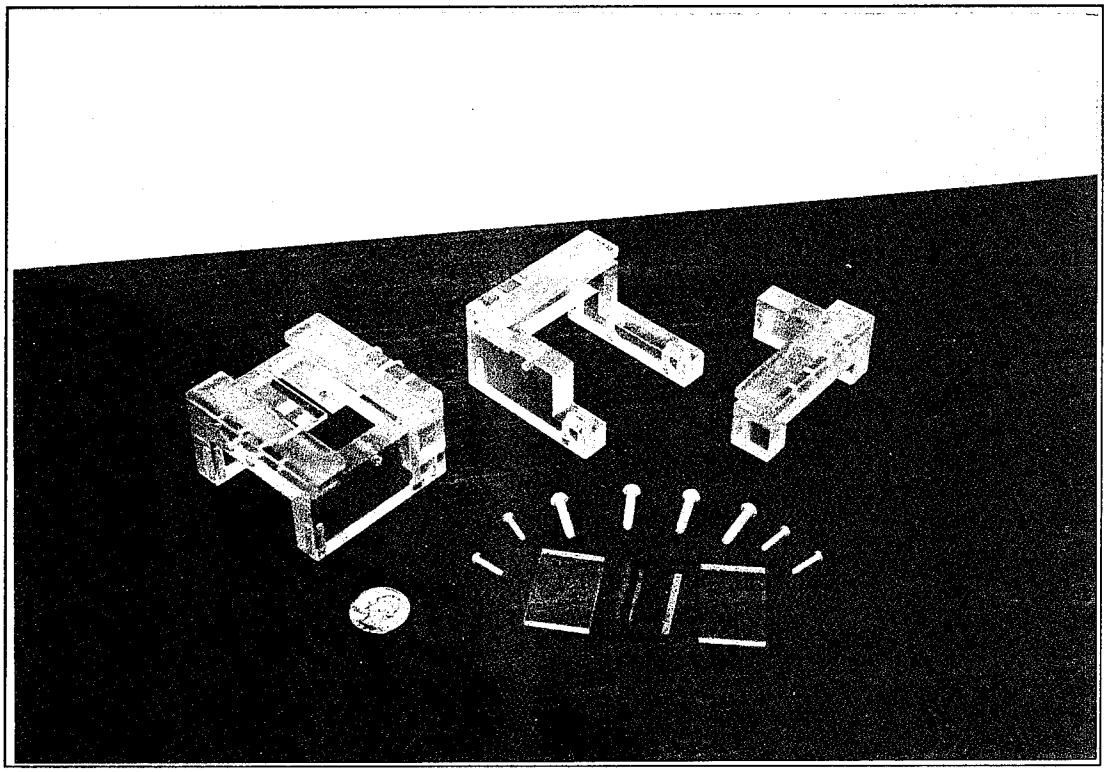


Figure 7: Photograph of the Plastic Crystal Mount. The assembled vise is shown at the left, while the vice parts, the copper tube, and the lithium tantalate crystal are at the right.

The completed tube was then carefully placed over the electro-optic crystal and the tube was gently pinched, holding the crystal between the tabs so that the crystal and the tube longitudinal axes remained parallel. Then the tube and crystal were mounted between two pieces of low-dielectric loss plastic which maintained the

compression between the tabs and the crystal through the use of nylon screws. A photograph of our plastic crystal mount is shown in Figure 7. A piece of rigid coaxial cable was passed through a hole in the crystal mount. A short loop of wire was soldered to this cable to form the antenna. The loop was formed by first bending two right angles in the wire which would fit around the crystal and the tabs on the tube (again, see Figure 5). Then the wire was wrapped around a drill bit that was larger than the one used to form the copper tube, and the loose ends were bent so that they would mate with the rigid coaxial cable. The entire crystal mount assembly was then housed inside of a grounded, aluminum shielding box which had pre-drilled holes to allow the laser beam to pass through the box.

With the modulator crystal and the laser source completed all that remains is to characterize the RF source. The modulating RF frequency is provided by an Avantek VTO 8240, a varactor-tuned oscillator capable of producing frequencies from approximately 2.4 to 3.7 GHz. The VTO is a small chip which is mounted in a project box to better control its thermal environment, since the output frequency depends on the chip temperature. The VTO output signal was fed into an impedance-matched power divider, where it was directed to a microwave frequency counter which monitored the frequency, and to a Mini-Circuits ZHL-42 High Power Amplifier. The power divider stepped the VTO's output of 10 dBm down to about 4 dBm, a level which the amplifier could handle. The amplifier increased the signal to about 25 dBm

(about 300 mW), which was then fed into the EOM antenna. It is critical at these frequencies that the cable lengths between devices is kept to a minimum. As an example, at 3 GHz, the attenuation of the RG-178 cable we used is about 85 dB per 100 feet.[27]

This concludes the physical descriptions of the important apparatus used in this experiment. In the next chapter we will chronicle the testing and evaluation of this equipment and then begin to describe the actual experiments that demonstrate some of the first sucessful steps toward the ultimate goal of coherent excitation.

CHAPTER FOUR: EXPERIMENTAL PROCEDURE

The experimental portion of this project consisted of two relatively independent sections. After the relatively complicated pieces of equipment described in the previous chapter had been constructed and assembled, the next step was to characterize their operation. The first section of this chapter deals with that subject. Once we could predict what the outcome of changing critical parameters on this equipment would be, it became possible to apply the devices to more fundamental physical problems.

EQUIPMENT EVALUATION

Before any work could be done with the electro-optic modulator, the grating tuned laser had to be made operational. After all the components had been assembled, testing of a particular diode laser began by characterizing its free-running qualities. A high-quality mirror was substituted for the grating and, as in the collimation procedure, the laser was focused on the far wall. The beam shape was observed to be roughly elliptical with an aspect ratio of approximately six to one. The quality of

the elliptical pattern was the cause for some worry, however, since the intensity distribution was not as smooth as other diode lasers. Next, the beam was directed at a power meter and data were taken to determine the power vs. injection current response of the diode. A scanning Fabry-Perot cavity spectrum analyzer showed that the free-running laser linewidth was on the order of 30-40 MHz. When the grating was substituted for the mirror and similar data were taken, the power dropped by about one-third. Plots of the power/current data for both the free-running and grating modes are presented in Figure 8. For both cases, the threshold was determined to be about 46 mA. It is important to note that for these measurements, the laser was not operating in a grating-locked mode, and that the power output increases and the threshold decreases significantly under a feedback locking condition.

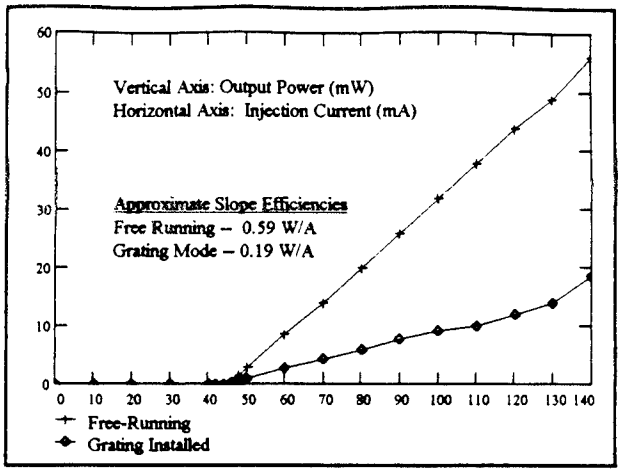


Figure 8: Laser Output Power vs. Injection Current. Data for the Hitachi HL7851G laser diode.

Next, the grating tilt was carefully adjusted until the first order diffraction maximum was directed back into the lens. By using an infrared viewer focused on the grating, it became obvious when the laser began to operate in the feedback mode. With small adjustments of the grating tilt screws, a discrete, very noticeable

brightening of the cavity indicated that the grating was indeed providing feedback to the laser. The grating-tuned linewidth was not precicely determined, but it did reduce to below 25 MHz, the resolution limit of our spectrum analyzer.

To evaluate the stability of the lock, the output beam was redirected into the spectrum analyzer. It was determined that the temperature and current response of the laser frequency was unchanged, i.e. the laser frequency could be easily and continuously tuned by adjusting either of these parameters, definitely not a desired result for a well-designed grating-tuned laser. However, by adjusting the voltage on piezo-electric cylinders which vary the external cavity length and the angle of the grating, it was possible to tune the laser frequency over 15 GHz before a mode hop occurred. As the relevant absorption spectrum of ^{85}Rb is only about 3 GHz wide, this tuning range was more than adequate. For our piezos, we found a tuning relationship between piezo voltage and laser frequency of 30 MHz per volt. Thus, we were able to tune the laser to near the center of the rubidium absorption spectrum using small current and temperature adjustments, and then scan the laser across all four absorption lines by slowly ramping the voltage on the piezo-electric cylinders. The bottom line is that we have an operable grating-tuned laser with a poor or non-existent lock.

The EOM was evaluated in several stages. First, the spectrum of the RF oscillator was examined. The fundamental frequency from the oscillator was a large, approximately Lorentzian peak with a width of only about 50 kHz. Several sidebands

were present, as well as numerous harmonics and subharmonics. The strongest of these secondary frequencies was the first harmonic, but its intensity was over 13 dB down from the primary signal. The sidebands were all over 60 dB lower than the carrier. Thus, the only significant frequency coming out of the oscillator was the carrier.

The oscillator frequency exhibited a reasonably strong temperature dependence of -0.4 MHz per Kelvin. However, the temperature of the VTO quickly reached an equilibrium value of 1.5 Kelvin above ambient temperature after only a 10 minute warm-up, and the frequency only drifted away from the equilibrium value by ± 10 kHz over an eight hour period. During operation, the VTO output frequency is primarily tuned by adjusting a tuning voltage between 1 and 45 volts. A plot of this tuning relationship is shown in Figure 9.

The oscillator was then connected to the EOM antenna by way of the amplifier. Between the antenna and the amplifier we placed an isolator/circulator combination which served two purposes. Since the impedance of the antenna could not be properly matched to the rest of the circuit, the isolator prevented damaging voltage oscillations from returning to the amplifier. The circulator allowed us to monitor the reflected power from the antenna as a resonance diagnostic. The isolator/circulator provided over -37 dB protection to the amplifier at 3.0 GHz.[28]

Using the diagnostic port on the circulator, we again examined the oscillator

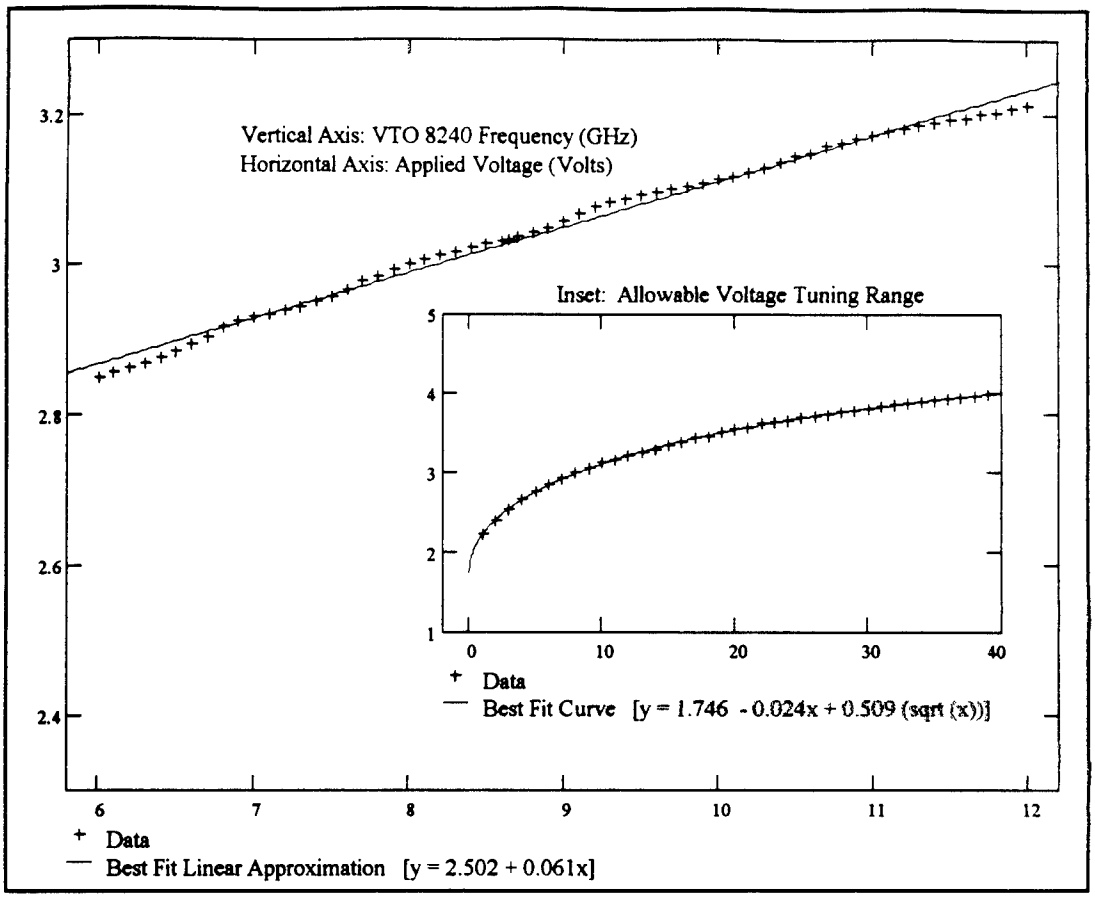


Figure 9: RF Oscillator Frequency vs. Tuning Voltage. The graph shows the approximately linear region used in the experiment, while the inset shows the oscillator's useable range.

frequency spectrum, this time looking at the spectrum of the reflected power while the EOM was not on resonance. We found similar results to those above, the fundamental frequency was the dominant output, but the amplifier had filtered out most of the higher order overtones so that now the intensity of the next noticable frequency was over 34 dB down from the fundamental.

Next the grating-tuned laser and the EOM were combined. As seen in Figure 10, there were several components besides just the two primary pieces of equipment

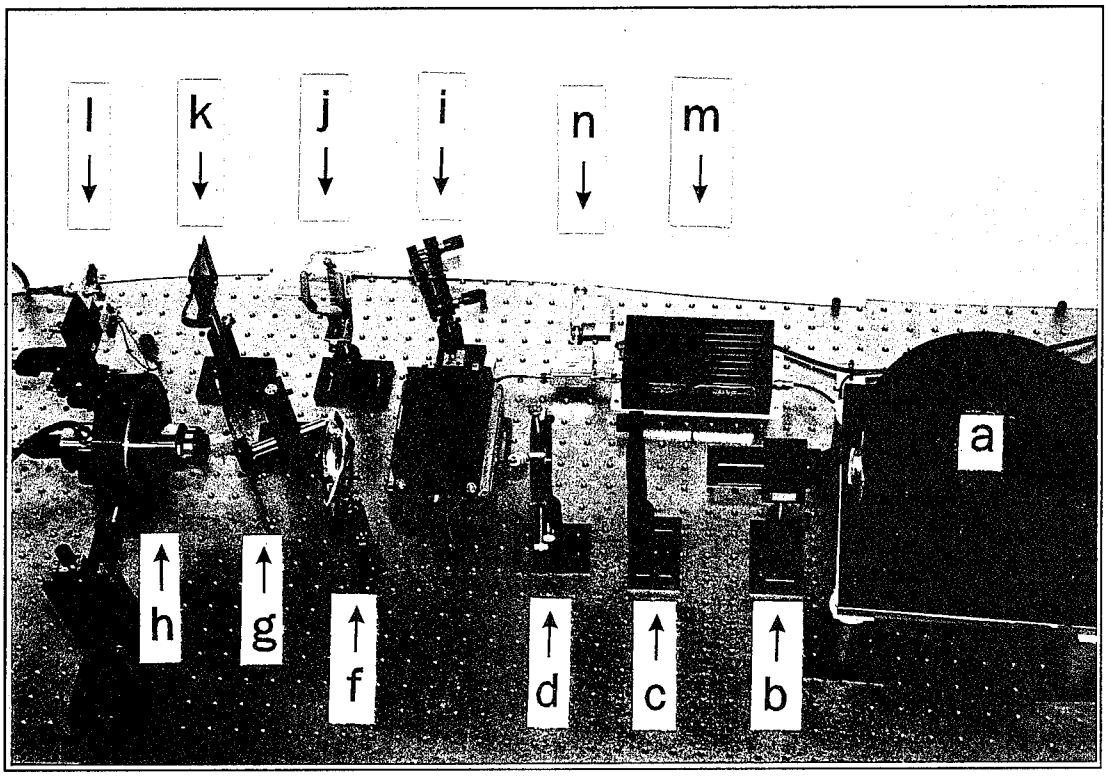


Figure 10: Photograph of The Experimental Setup. For scale, the holes on the optics table are one inch apart. See text for further description.

already described that were required to generate sidebands on the laser beam. At the far right is the grating-tuned laser (A). the output beam passes through an optical isolator (B) to prevent additional external cavities from resonating, and then through a half-wave plate (C). The $\lambda/2$ plate rotated the polarization direction so that it was properly aligned on the crystal to provide the maximum modulation index. Next, the beam passes through a lens (D) which focuses the laser beam on the EOM crystal inside the grounded shielding box (E); a second lens (F) then recollimates the beam before it passes through a variable beam splitter (G) on its way to the spectrum

analyzer (H). The fraction of the light which is not passed by the variable beam splitter reflects off a mirror (I) prior to passing through a glass cell filled with atomic rubidium vapor (J) and a neutral density filter (K) on its way to a photodiode (L). The RF amplifier (M) and the isolator/circulator (N) are also shown.

Once the equipment was arranged it was a relatively simple matter to begin looking for sidebands. The laser was turned on and the beam splitter was adjusted so that most of the light went into the spectrum analyzer. For two reasons we initially decided to look for decreases in the carrier intensity instead of looking directly for the sidebands. For the small preliminary modulation indices that we expected to achieve, the sidebands themselves might be so small that they would be lost in the noise level of the analyzer. Also, the loss in the carrier intensity would be twice as pronounced as the change in the height of a single sideband, so we got a built-in factor of two increase in our ability to detect a resonance. We then slowly tuned the RF oscillator across its frequency range and monitored both the optical spectrum analyzer display and the spectrum of the reflected power from the EOM antenna.

After several unsuccessful tries, we finally found a combination of antenna shape, antenna position, and tube size which produced small but noticeable sidebands at approximately 3.5 GHz. The sideband intensities were only about 5% of the carrier, but slight adjustments of the antenna position increased this value to about 20%. The optimum antenna position was easily determined by monitoring the

reflected power; when the critical coupling position was reached, the reflected power fell by approximately 15 dB compared to its over- and undercoupled values.

A little more experimentation with this particular setup yielded several interesting observations. Contrary to previous reports[29], we found that the placement of metal objects near the crystal box did not have a noticeable effect on the resonant frequency of the crystal, even when the top of the box was removed. Furthermore, we found that the amplitude of the sidebands increased by factors of three to five when the EOM was shielded on all sides, i.e. when the shielding box top was in place. We attribute this to the fact that the length of our shielding box is on the order of $\lambda/2$ (the box measures 5 x 9 x 11.5 cm), and thus the complete shielding box formed a low-Q resonant cavity, allowing more RF energy to be available to resonate in the LRC circuit.

The initial diameter of our tube was based upon finding the radius that would give a resonant frequency at 3.035 GHz from equation 6. The approximations previously mentioned, along with the imprecise construction methods used to manufacture the tube caused this predicted frequency to be lower than the observed frequency. The frequency was close enough, however, to continue to use the equation as a good first approximation. During our tuning efforts, we also discovered that each of these tubes exhibited not one but two resonance frequencies. Since our resonant frequency prediction relied on the assumption of a perfect cylindrical form for our

tube, it is not unreasonable to expect other resonances for the non-cylindrical form actually used. Both the resonances produced comparable sideband amplitudes. It is possible to fine-tune the resonance of the LRC circuit by slightly deforming the copper tube. This tuning method was very effective for small (10-20 MHz) shifts in the circuit's natural frequency; however, we found that deforming the cylinder enough to shift the natural frequency by over 50 MHz resulted in a greatly reduced cavity Q value, and hence greatly reduced sideband amplitudes. Thus, our gross tuning method consisted of constructing new tubes of differing diameters. In all, we made six tubes before we found the correct diameter. Data concerning these tubes and their resonant frequencies are presented in Figure 11, and the data seem to support the 1/r relationship from equation 6.

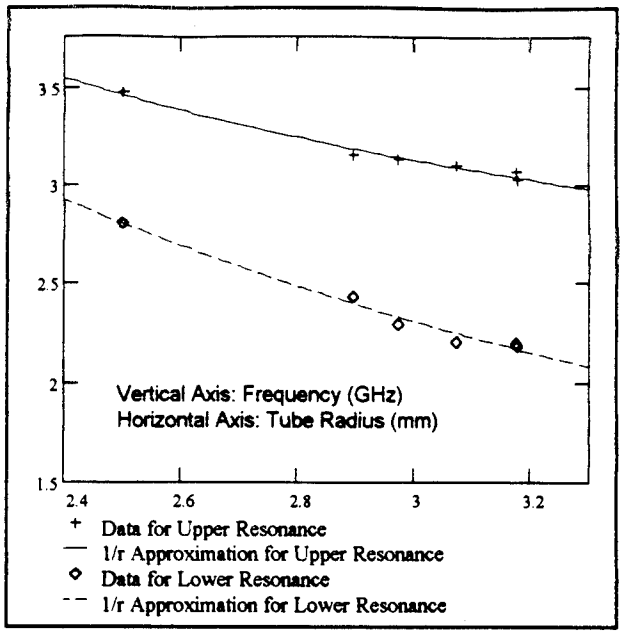


Figure 11: Tube Size vs. Resonant Frequency. The data support the theoretical 1/r relationship.

Once we constructed a tube which had a natural frequency near the desired value, we adjusted the antenna position and the resonant frequency until the EOM produced large sidebands at exactly the ^{85}Rb ground state frequency split. One optical

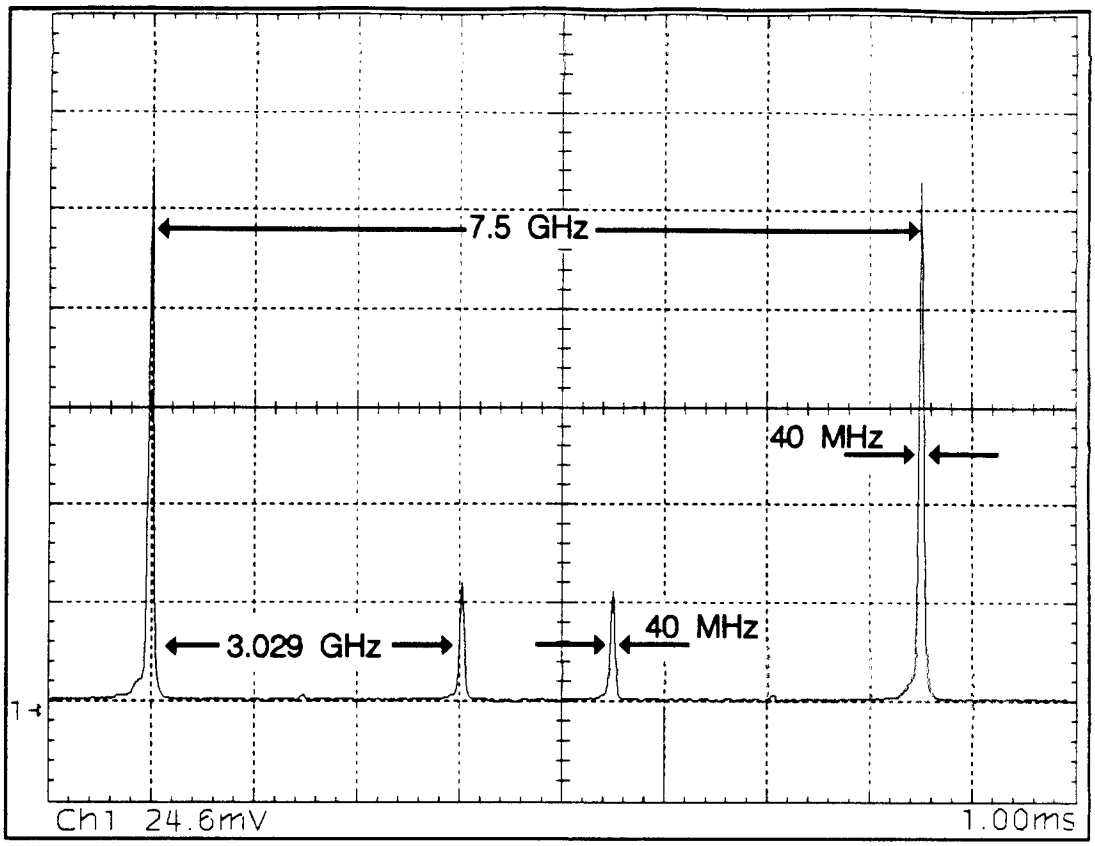


Figure 12: Optical Spectrum Showing the Laser Carrier and Sidebands.

spectrum from this resonator is shown in Figure 12. The full width at half maximum (FWHM) for each of the peaks is indicated on the figure. The intensity of the first-order sidebands are approximately 21% of that of the carrier, implying a modulation index of about 0.8. Small second-order sidebands can just be seen a little more than 6 GHz. from each of the carriers. The width of the sidebands is dependent upon the carrier width in this presentation; it has no bearing on the width of the resonance itself, which is a function of the Q of the cavity. By slowly tuning the voltage on

the oscillator, noting the amplitude of the sideband, and converting the voltages into frequencies, we determined that the resonance width of this LRC circuit was only 15 MHz. Since $Q = \omega_0 / \Gamma$, where ω_0 is the oscillator frequency and Γ is the FWHM of the resonance, then the Q of this EOM is on the order of 200.

The last characteristic of the EOM that we investigated was the warm-up time. We have already noted that the RF oscillator had a temperature dependence; it turns out that the EOM also has such a dependence. As the LRC circuit begins to resonate, the inherent resistance in the copper tube causes the tube to heat up slightly. This heating causes the resonant frequency of the EOM to fall slightly. Figure 13 shows the exponential decrease in the resonant frequency as a function of time. For the data, all components in the EOM and the grating-tuned laser were allowed to warm up for about an hour. During this time, the laser was on and directed through the $LiTaO_3$ crystal. At time t = 0, the oscillator was connected to the amplifier and was immediately tuned to resonance. During data collection, the EOM was retuned to the point where maximum sideband intensities were generated every minute. As can be

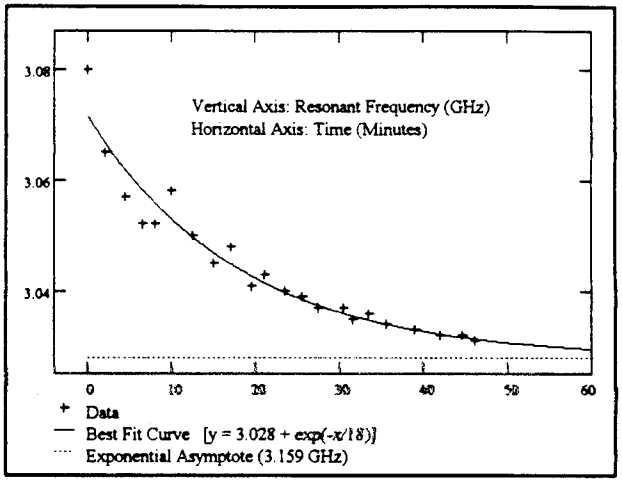


Figure 13: Time Dependence of EOM Resonant Frequency.

seen, the resonant frequency stabilized to within 2 MHz of its asymptotic value after about a one hour warm-up.

THE SIMULTANEOUS PUMPING EXPERIMENT

Now that the equipment has been designed, tested, and characterized, we can refocus our attention on the atomic physics that got us started down this track in the first place. Our goal was to stimulate both states in the hyperfine doublet of rubidium-85. In order to show that our set-up was able to do this, we decided to look first at the rubidium absorption spectrum. As was seen in Figure 10, the laser was directed at a variable beam splitter which allowed part of the beam to go to a spectrum analyzer and shunted the rest of the beam through a rubidium cell. By placing a photodiode directly in the beam after the cell and monitoring the intensity of light as a function of frequency, it is relatively easy to identify the frequencies where the photodiode signal drops abruptly due to the absorption of the rubidium atoms. Each frequency corresponds to an area where the rubidium atoms in the cell are able to resonantly absorb the light. The photodiode signal drops in these areas because some of the excited rubidium atoms relax back to their ground states through fluorescence, that is, by spontaneously emitting photons in random directions. The vast majority of these photons do not reach the photodiode, so the photodiode signal

falls off.

Above a certain radiation intensity, known as the saturation intensity, very little further absorption can occur, as almost all of the atoms within the beam are already being driven between the excited state and the ground state in what are known as Rabi cycles. Atoms undergoing Rabi oscillation above the saturation intensity do not detract from the photodiode signal because although photons are being absorbed by ground state atoms, the excited state atoms relax by way of stimulated emission, emitting a photon in the same direction as the photon that stimulated the relaxation; for almost every absorption there is now a corresponding emission.

The normal rubidium spectrum is shown in Figure 14. All of the following traces were taken at laser intensities below saturation (the beam diameter was about 5 mm and the output power was about 1 mW). For this trace, the frequency of the laser was swept by applying a ramp to the laser injection current. As the injection current increases not only does the lasing wavelength increase, but the laser intensity increases as well. The absorption dips are

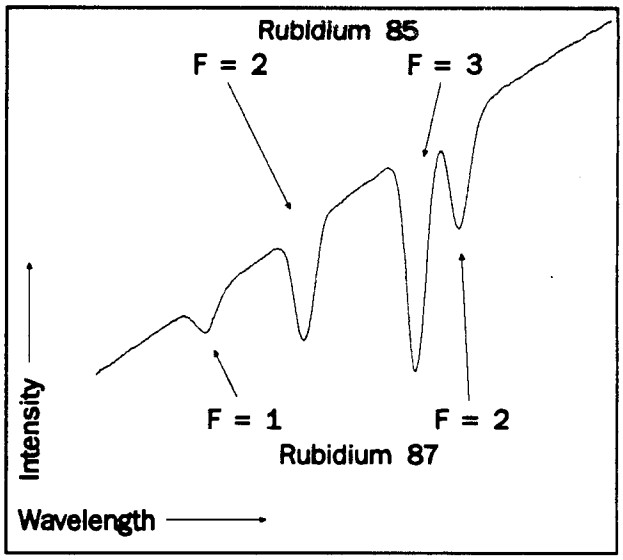


Figure 14: The Rubidium D_2 Absorption Spectrum. Note that frequency *decreases* from left to right.

not infinitely sharp spikes that correspond to single absorption frequencies, but have a finite width that depends on numerous broadening mechanisms. The resonances have different depths due to several factors. There are 2F+1 sublevels for each of the m_f levels shown in Figure 14. Thus, for an equilibrium sublevel population, the F=2 sublevel contains 5/12 of the ^{85}Rb atoms and the F=3 sublevel contains the remaining 7/12 of the population. Since more atoms are available to absorb at the frequency corresponding to F=3, the resonance is more pronounced. The discrepancy between the depth of the ^{85}Rb and ^{87}Rb F=2 resonances is due to the 72:21 ratio of the natural isotope abundances.

In the above discussion of absorption and saturation we were referring only to one transition at a time. When the laser is tuned to, say, the ^{85}Rb F=2 transition, the atoms that were originally in the F=3 sublevel are not affected. If we can simultaneously stimulate the other level, the overall absorption (which would then be due to *both* the F=2 and F=3 transitions) should increase because there are now more atoms available to absorb photons. This was the hypothesis for our experimental setup.

For the actual experiment, the laser frequency was not scanned. The grating position was slowly adjusted until a sharp decrease in the photodiode signal was noted. By sequentially tuning across all four lines it was possible to accurately identify the exact transition we were stimulating. Initially we tuned the laser to the

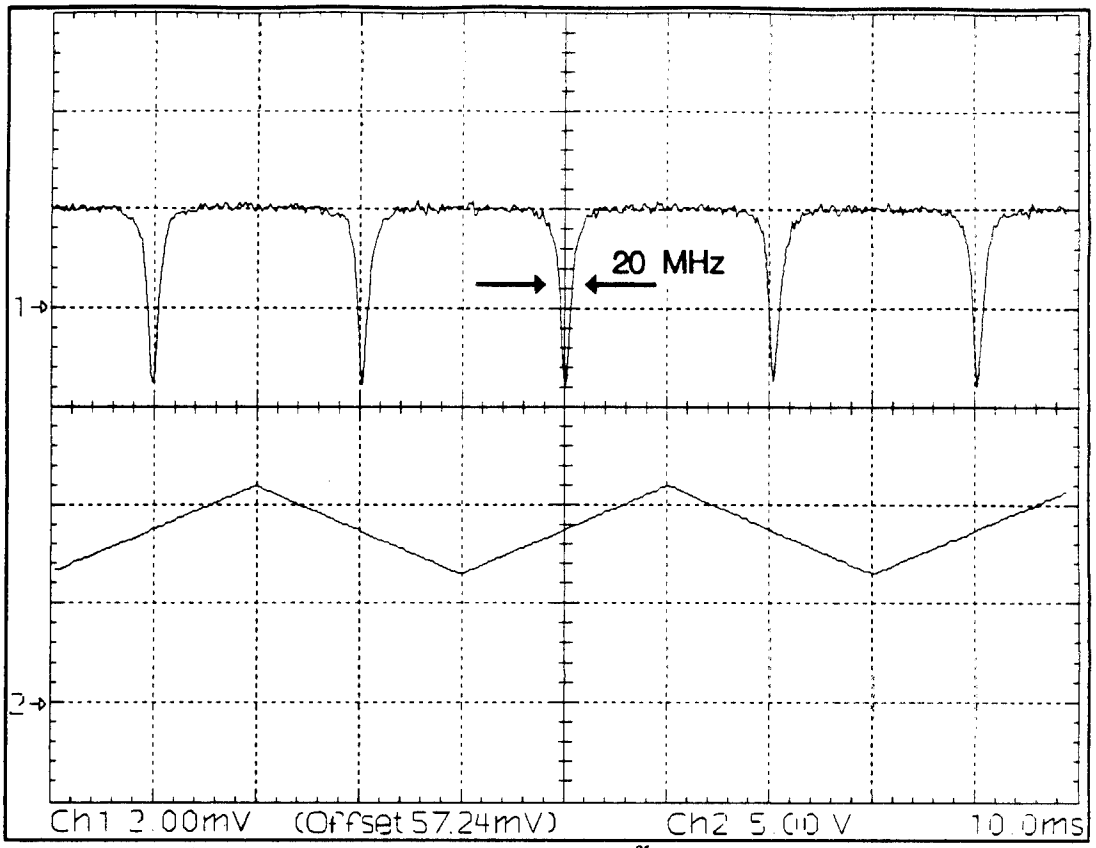


Figure 15: Simultaneous Absorption While Tuned to the ^{85}Rb F=2 Transition. The FWHM of the area of increased absorption is 20 GHz.

^{85}Rb F=2 transition. We then drove the oscillator tuning voltage with a sawtooth wave from a function generator at 25 Hz. The center frequency of the tuning voltage ramp was 8.75 V and the amplitude of the ramp was 2.26 V. Referring back to Figure 9, this converts into a frequency scan of 2.890 GHz to 3.175 GHz, centered at 3.040 GHz.

Figure 15 shows the trace taken with this setup. The sharp dips in the trace are centered at 3.029 GHz, the EOM resonant frequency, and are 3.57 mV deep and

20 MHz wide. The portion of the trace where the sidebands are not being generated is at a level of 59.24 mV, while the zero-absorption signal level (not shown) is 126.2 mV. Thus, absorption of the carrier alone causes a 66.96 mV drop in the photodiode signal and the addition of the sidebands adds another 5.3% to that signal drop.

The explanation of these results is relatively straightforward. As the oscillator frequency drives the EOM resonance, sidebands are written on the laser beam. Although the sidebands decrease the intensity of the carrier that is driving the F=2 transition, the decrease in absorption is more than compensated by the absorption that occurs when the lower sideband begins to drive the F=3 transition. In this particular case, the upper sideband is also able to be absorbed by the ^{87}Rb F=1 transition.

A similar trace (Figure 16) was obtained when the carrier was tuned to the ^{85}Rb F=3 transition. In this case, the upper sideband drives the F=2 transition but the lower sideband is not absorbed at all. On this trace, the carrier absorption signal level is 41.7 mV, the zero-absorption signal level (not shown) was 171.8 mV, and the sharp feature has a width of 20 MHz and a depth of 3.07 mV. Thus, the sidebands only increase the absorption by 2.4% in this case.

When the carrier is tuned slightly above the ^{85}Rb F=2 resonance, a different trace results. Figure 17 shows a point where the carrier is still within the F=2 absorption region, but the sidebands no longer map onto the ^{85}Rb F=3 nor the ^{87}Rb

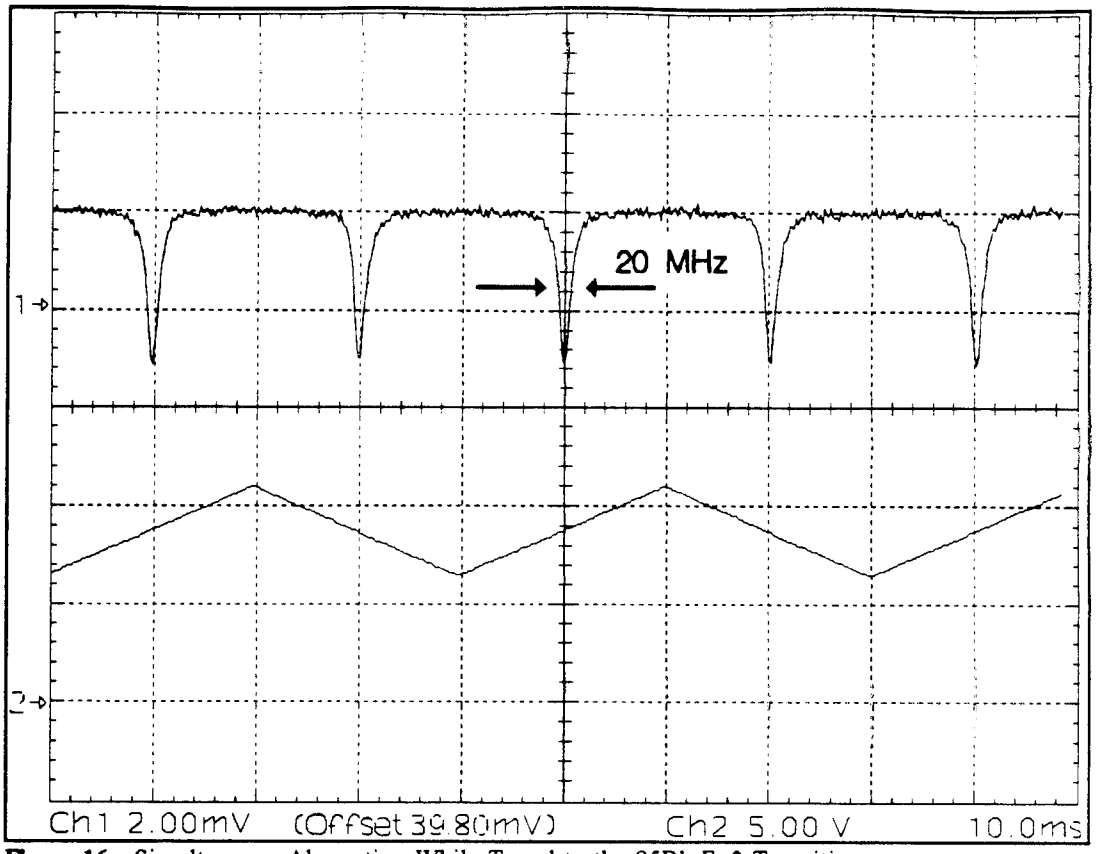


Figure 16: Simultaneous Absorption While Tuned to the 85Rb F=3 Transition.

F=1 resonances. Here, when the EOM is brought on resonance, the total absorption decreases sharply due to fact that the sidebands cause the carrier intensity to decrease while the light in the sidebands is not absorbed by any rubidium resonance. In this figure, the carrier absorption signal level is 33.88 mV, the zero-absorption signal level (not shown) is 148.9 mV, and the peak is 15 MHz wide and 2.43 mV deep implying a 2.1% decrease in the total absorption.

A different view of the simultaneous absorption phenomenon is presented in Figure 18. For this trace, the injection current to the laser was ramped, causing the

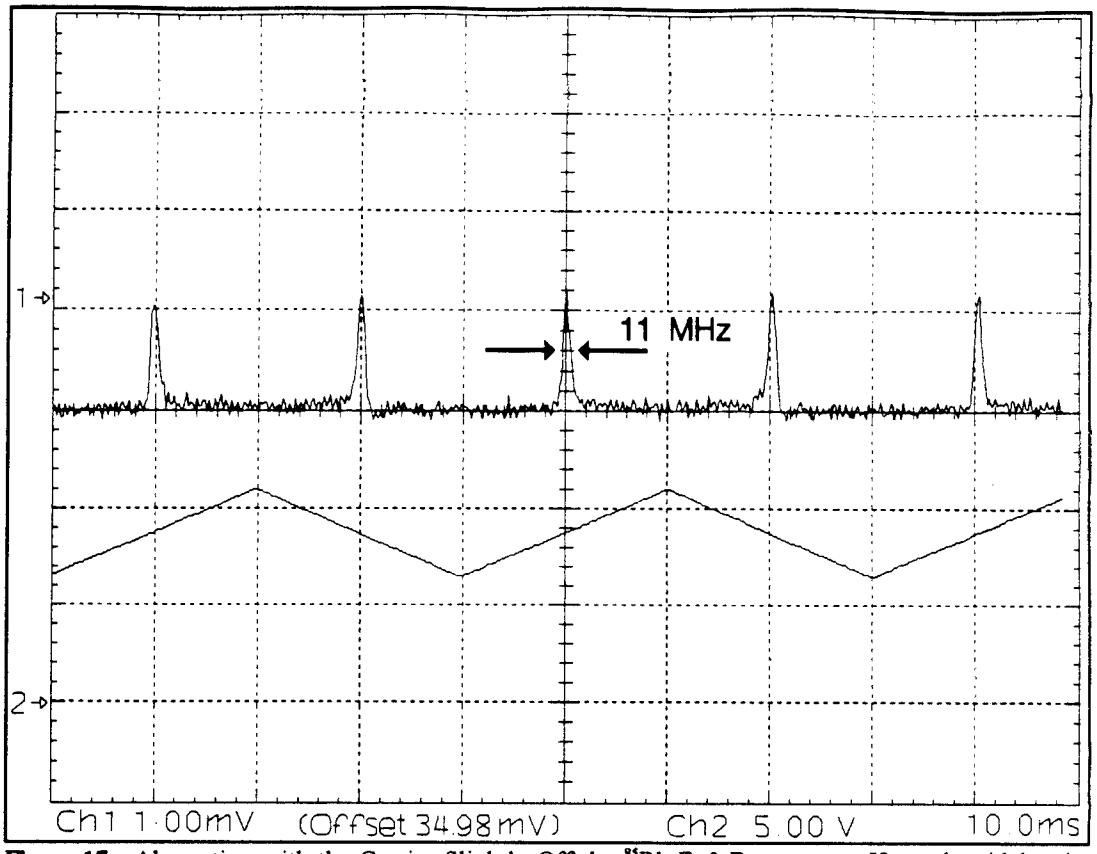


Figure 17: Absorption with the Carrier Slightly Off the ^{85}Rb F=2 Resonance. Here, the sidebands do not stimulate any transitions and are thus not absorbed.

distinctive upward intensity slope of the base line in the graph. The resonances numbered 1 through 4 are the usual spectrum associated with the ^{87}Rb F=1, ^{85}Rb F=2, ^{85}Rb F=3, and ^{87}Rb F=2 transitions, respectively. The lettered resonances are associated with the spectrum resulting from tuning the EOM to produce maximum sidebands and then ramping the carrier frequency. The explanation of this trace is simply a matter of mapping the carrier and sideband positions onto the no-sidebands spectrum, recalling that the carrier-sideband frequency difference was designed to

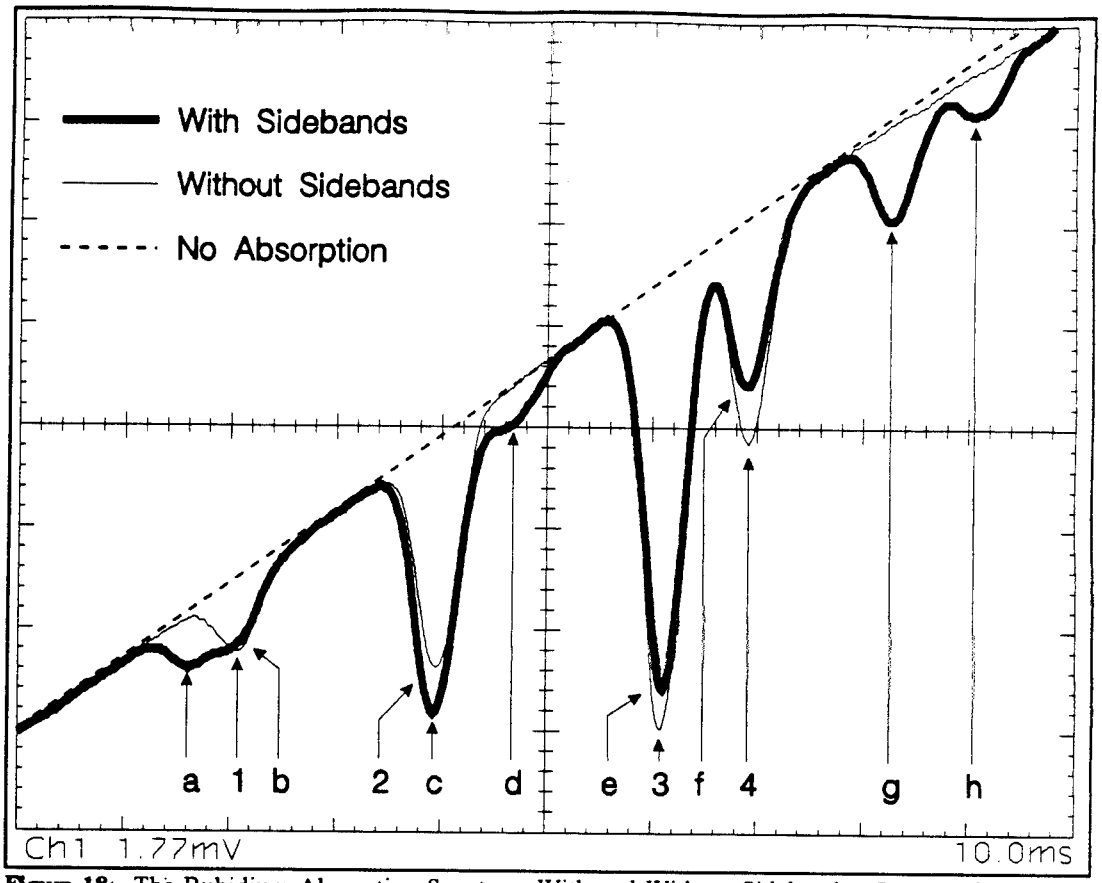


Figure 18: The Rubidium Absorption Spectrum With and Without Sidebands. See text for explanations of the various resonances. Note that frequency *decreases* from left to right.

exactly match the frequency split between peaks 2 and 3. Peak "a" occurred when the lower sideband was absorbed by resonance 2. Peak "b" is simply the carrier aligning with 1, and its decreased magnitude with respect to the no-sidebands trace is due to the fact that the sidebands are not absorbed by a resonance. Peak "c" is the carrier mapping to resonance 2. Its magnitude is due to the fact that both sidebands and the carrier are being absorbed, with the lower sideband being preferentially absorbed due to the fact that the F=3 sublevel population of resonance 3 is greater than that of the

F=2 sublevel population of resonance 2. Resonance "d" occurs when the lower sideband maps onto resonance 4. Peak "e" is again due to multiple absorptions. Here, the carrier is absorbed by resonance 3 and the upper sideband is absorbed by peak 2. However, the lower sideband passes through the cell unabsorbed. This lack of absorption combined with the sublevel population disparity mentioned above cause the with-sidebands peak to be diminished with respect to the without-sidebands peak. Resonance "f" is due to the carrier's absorption by 4 with no simultaneous absorption by either of the sidebands. Resonances "g" and "h" occur when the upper sideband maps onto 3 and 4, respectively. The trace was not expanded enough to show the absorption dip that occurred when the lower sideband stimulated the ^{87}Rb F=1 transition. That dip would be to the left of peak "a".

These results clearly demonstrate that we have achieved an important first step toward coherent excitation. We can definitely stimulate both hyperfine levels of rubidium-85 with one laser source. We are also probably generating a coherent excitation that occurs with a periodicity related to the beat frequency of the Rabi frequencies of the two individual levels with this experimental setup, although our data by no means show that effect. A possible experiment that could demonstrate just such a coherence is described in the following chapter.

CHAPTER FIVE: FUTURE WORK

Although we have come a long way from just directing a laser through a rubidium cell, much work remains to be done to follow up on these results. There are a number of interesting effects which remain to be explored.

Experiments that would directly show coherent effects include tuning the laser and sidebands to cause simultaneous absorption, and then sweeping the laser power while monitoring the absorption of a weak probe laser tuned to the carrier frequency. Modulating the laser power would change the hyperfine levels' Rabi frequencies and would change the resulting beat frequency. When the Rabi frequencies were in phase, i.e. when coherent excitation was occurring, the absorption should drop sharply. This is because the rubidium atoms then exist in the coherent superposition of the hyperfine ground states with an energy somewhere between the ground states. This energy level would not be stimulated by the probe, so the light would pass through the cell unabsorbed.

Unfortunately, our current laser lacks a strong frequency lock, so we are currently unable to modulate the power while maintaining a set frequency. External cavity lasers employing the Littman design mentioned in chapter three have

demonstrated a much stronger ability to frequency lock, and stable locks have been demonstrated on a high-power laser diode array from the laser threshold to approximately 1.5 Watts of output power.[30] With such a laser, it could be possible to not only sweep the laser power while maintaining a set frequency, but much higher powers could also be reached where definitive coherent effects might be observed.

This is only one of many possible paths down the road toward coherent excitation. The answers to a wide variety of basic physical problems as well as numerous, potentially very profitable applications lie only a short distance further down this path and are available to those with the energy to pursue them.

BIBLIOGRAPHY

1. W. F. Buell, "Semiconductor Laser Experiments with Rubidium Vapor with Applications to Fundamental and Applied Physics", Doctoral Dissertation, The University of Texas at Austin, 1994, p. 136.

2. Marlan O. Scully, "From Lasers and Masers to Phaseonium and Phasers", Physics Reports **219** (3-6), pp. 192-196 (1992).

3. J. D. Jackson, *Classical Electrodynamics*, 2d Ed., John Wiley and Sons, New York, 1975, pp. 285-286.

4. Scully, pp. 200-201.

5. Buell, pp. 5-6. Note the sign discrepancy on the injection current tuning coefficient. Dr. Buell uses the convention that the injection current is a negative quantity. We have chosen to use a more practical definition. As the *magnitude* of the injection current (as read on any commercial current supply) is increased, the lasing frequency decreases.

6. G.P. Agarwal and J. T. Klaus, "Effect of Phase Conjugate Feedback on Semiconductor Laser Dynamics", Opt. Lett., **16**(17), 1325 (1991).

7. F. A. Jenkins and H. E. White, *Fundamentals of Optics*, 4th Ed. , McGraw Hill, New York, 1976, pp. 375-376.

8. K. Liu and M. G. Littman, "Novel Geometry for Single-Mode Scanning of Tuneable Lasers", Opt. Lett. **6**, 117 (1981).

9. P. McNicholl and H. J. Metcalf, "Synchronous Cavity Mode and Feedback Wavelength Scanning in Dye Laser Oscillators with Gratings", Appl. Opt. **24** (17), 2757 (1985).

10. T.F. Gallagher et. al., "Principles of a Resonant Cavity Optical Modulator", Appl. Opt. **25**(4), 510 (1986).

11. W. N. Hardy and L. A. Whitehead, "Split-Ring Resonator for Use in Magnetic Resonance from 200-2000 MHz", Rev. Sci. Instrum. **52**(2), 213 (1981).

12. J. F. Kelley and A. Gallagher, " Efficient Electro-Optic Modulator for Optical Pumping of Na Beams", Rev. Sci. Instrum. **58**(4), 563 (1987).

13. Gallagher , p. 510.

14. I. P. Kaminow, *An Introduction to Electrooptic Devices*, Academic, New York, 1974.

15. L. B. Arguimbau and R.D. Stuart, Frequency Modulation, John Wiley & Sons, London, 1956, pp. 7-22.

16. Kaminow, p. 213.

17. Kaminow, p. 213.

18. P.V. Lenzo *et. al.*, "Electrooptic Coefficients and Elastic Wave Propagation in Single Domain Ferroelectric Lithium Tantalate", Appl. Phys. Lett. **8**, 81 (1966)

19. R. A. Stolzenberger of Crystal Associates, Inc., 15 Industrial Park, Waldwick, NJ 07463, private communication.

20. T. Day of Nu Focus, 1275 Reamwood Ave., Sunnyvale, CA 94809, private communication.

21. R. Luttge of Crystal Technology, Inc., 1040 E. Meadow Cir., Palo Alto, CA 94303, private communication.

22. Gallagher, p.510.

23. Kelley, p. 564.

24. Kaminow, p. 167.

25. Kelley, p. 564.

26. Kelley, p. 565.

27. John H. Moore, Christopher C. Davis, and Michael A. Coplan, *Building Scientific Apparatus: A Practical Guide to Design and Construction*, 2d Ed., Addison-Wesley, Reading, Mass., 1989, p. 377.

28. T. Rodriguez and J. Mitchell, Sierra Microwave Technology, 1 Sierra Way, Georgetown, TX 78626, private communication.

29. Kelley, p.566.

30. J. Sabbaghzadeh, "A Highly Sensitive Spontaneous Raman Spectrometer for the Determination of Concentrations in Gas Mixtures", 1993, unpublished.

VITA

Edward Brown Tomme was born in Fort Worth, Texas on 27 February 1963, the son of Anne Lege Tomme and Marion Brown Tomme, Jr. After graduating as the valedictorian of the Class of 1981 at Arlington Heights High School, Fort Worth, Texas, he was appointed to the United States Air Force Academy. He received the degree of Bachelor of Science with honors from The Air Force Academy and was recognized as a Distinguished Graduate of the Class of 1985, the Academy's version of *Magna Cum Laude*. Following his commissioning as a Second Lieutenant in the United States Air Force, he went on to pilot training in Lubbock, Texas, where he met and married his wife, the former Tracey Lynn Arnold. He has flown a variety of aircraft including the T-37 Tweet, the T-38 Talon, the F-4E Phantom II, and the F-4G Wild Weasel during tours of duty in the United States, Germany, and the Persian Gulf. Captain Tomme was selected by the Air Force to attend The Graduate School at The University of Texas at Austin in January, 1993, in preparation for an assignment as an Instructor of Physics at the United States Air Force Academy.

Permanent Address: 6833 Middle Road

Fort Worth, Texas 76116